small NANO MICRO

Humidity Sensors

Modulation of Electron Tunneling in a Nanoparticle Array by Sound Waves: An Avenue to High-Speed, High-Sensitivity Sensors

*Vikas Berry and Ravi F. Saraf**

Using an electrostatic self-assembly process, metal nanoparticles are deposited on polyelectrolyte fibers such that the interparticle distance between the nanoparticles is comparable to the polyelectrolyte's molecular width. By modulating the dielectric properties of the interparticle polymer layer, a highly sensitive, reversible humidity sensor with an ultrafast response time of ≈3 ms is demonstrated. The higher sensitivity at low humidity shows a conductivity increase by over two orders of magnitude in response to a change in relative humidity from 21 to 1%.

1. Introduction

Nanostructures, such as carbon nanotubes, silicon nanowires,[1–4] and metal and semiconducting nanoparticles,[5] are proving to be effective components to build stand-alone electronic devices with a broad range of potential applications, for example, biosensors,[6–10] logic circuits,[11–13] and hybrid devices with live cells.[14–19] The uniqueness in terms of novel functionality, sensitivity, and in some cases the ease of fabrication (compared to microelectronics) is quite evident. For example, by measuring the modulation of electrical properties, carbon nanotubes can measure the velocity of electrolytes,[20] operate as a logic device providing its own circuitry,[11–13] and make pressure-sensitive devices.[21] Recently, semiconducting nanowires (Si, ZnO, etc.) have also emerged as viable nanomaterials with unique applications, such as production of electrical energy by mechanical vibration,[22] detection of viruses[3,23] and other biomolecules,[3] and performance of logic operations.[24] For nanoparticle-based systems that possess similar distinctions of functioning as stand-alone electronic devices, such as a single-electron transistor[5,25] and electronic switch based on a negative-differential resistor,[26–28] the progress towards practical devices has been slower primarily due to the challenge of integrating them with conventional microelectronic circuitry. Self-assembled arrays of particles, on the other hand, have been developed to make a broad range of devices, for example, solar cells,[29,30] highly sensitive electronic devices on live bacteria,[14–16] a battery,[31] and an electronic skin with touch sensitivity comparable to that of the human finger.[32] For practical device applications, one-dimensional nanostructures, such as nanotubes and wire, have a distinct advantage in terms of integration with power and signal I/O (input/output).

Herein, we report an approach to fabricate an electrically conducting one-dimensional functional structure by self-assembling negatively charged Au nanoparticles on a positively charged polyelectrolyte microfiber. Because of interparticle repulsion between the similarly charged nanoparticles, a major challenge is to achieve close proximity for good electrical contact. The coulombic repulsion between the particles is overcome by charge compensation from positively charged poly(allyl hydrochloride) (PAH) deposited on the fiber. Furthermore, the thickness of the polymer layer between the nanoparticles is calculated to be ≈0.17 nm, which is close to the lateral thickness of a single polymer chain. The potential of the device is realized for its sensitivity to water adsorption and desorption on the molecular junctions between nanoparticles. Specifically, the device exhibits a reversible change in conductivity by over two orders of magnitude in response to a change in relative humidity (rH) from 21 to 1%. The high sensitivity is attributed to a) the charge-transport mechanism being electron tunneling, which has exponential dependence on the dielectric constant between

Prof. R. F. Saraf
Department of Chemical and Biomolecular Engineering
University of Nebraska–Lincoln, USA
E-mail: rsaraf@unlnotes.unl.edu
Prof. V. Berry
Department of Chemical Engineering
Kansas State University, USA

DOI: 10.1002/smll.201100519

nanoparticles, and b) the cumulative contribution of the over 10^3 nanoparticle–polymer–nanoparticle junctions in the percolating channel. Furthermore, since the change in conductivity is via a direct change in electron-tunneling barrier and not from a change in ionic-charge density or chemical gating, the device shows a much superior ultrafast response time of ≈3 ms, in contrast to 2–30 s for humidity devices based on ionic conductivity and chemical gating.

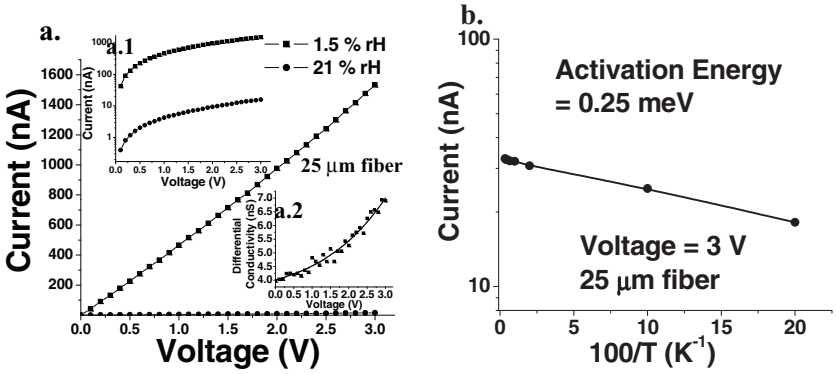

Figure 2. a) Current–voltage (I–V) behavior of a 25 μm fiber device, where voltage is increased from 0 to 3 V with a step size of 100 mV. The I–V results are shown at two humidity values (1.5 and 21% rH). Notice the small curvature in the curve. Insets: a.1) Log chart of I–V showing that the I–V behavior at the two humidity values is similar; a.2) differential conductivity of the device in nS, showing an increase in differential conductivity with voltage, which indicates the nanoparticle's coulomb blockade effect. b) Current versus temperature (100/T) data at 3 V bias for a 25 μm fiber device. The activation energy for electron transport of 0.25 meV indicates that electron transport is through electron tunneling.

2. Device Fabrication

The device is fabricated on a silica substrate with predeposited gold electrodes 7 μm apart. The silica substrate is cleaned and hydroxyl groups are introduced on the surface by oxygen-plasma treatment. Subsequently, the substrate is washed with *n*-octadecyltrichlorosilane for 2 h to deposit a hydrophobic monolayer on the silica surface. To make the gold surface hydrophobic, the substrate is washed with 1% dodecylthiol solution overnight. A 40% solution of positively charged polyelectrolyte PAH solution is then spun to make microfibers, which are placed across the electrodes on the hydrophobic substrate. The chip is subsequently baked in the presence of atmospheric oxygen for 6 h to bond the fiber to the silica surface. The baking step is crucial to avoid the PAH fiber being washed away during subsequent processing. Also, without the baking process, the fibers dewet forming chains of beads in 48 h. After baking, the chip is washed with deionized (DI) water to remove excess PAH. The excess PAH does not deposit elsewhere on the chip since all the other surfaces are hydrophobic. The remaining PAH on the surface forms stable fibers with excellent adhesion to the substrate. The substrate is finally immersed in negatively charged gold nanoparticle solution for 8 h to form an electrically percolating array of nanoparticles (**Figure 1**). As seen in Figure 1a, a multilayer deposit of nanoparticles is obtained, which indicates that the nanoparticles diffuse into the fiber. The deposition density after 8 h is ≈1000 nanoparticles μm^{-2}. The negatively charged nanoparticles are expected to crosslink the PAH in the fiber, thus making the device mechanically stable. Using this method, various devices with fiber diameters ranging from 1.5 to 25 μm were fabricated (see Figure 6 of the Supporting Information).

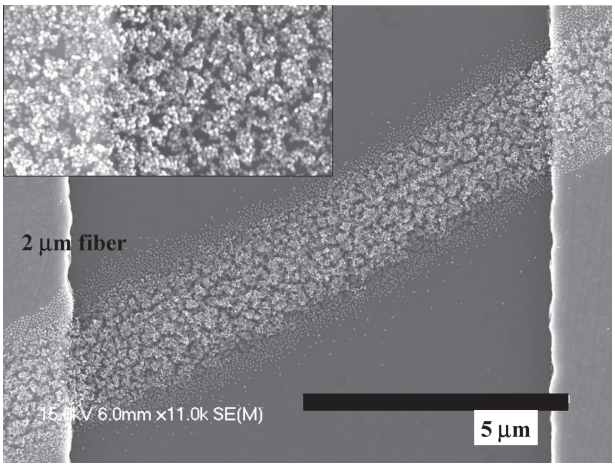

Figure 1. Scanning electron microscopy (SEM) image showing 30 nm gold particles deposited on PAH fiber 2 μm in diameter deposited across 7-μm-wide gold electrode pads. Scale bar: 5 μm. Inset: High-magnification SEM image of nanoparticles deposited on PAH fiber. The image shows that the deposition is percolating and the density is the same on the gold pad and silica.

3. Results and Discussion

A two-point conductivity measurement of a device with a 25 μm fiber between electrodes with voltage ramping from 0 to 3 V in step sizes of 100 mV shows that the device exhibits nominally ohmic current–voltage (I–V) characteristics at 21% rH (**Figure 2**a). Furthermore, it also exhibits a slight curvature in I–V behavior, which is attributed to local charging in the percolating channels that possess a coulomb blockade. This curvature is more exemplified in the differential conductivity of the device (inset, Figure 2a.2). Interestingly, the device undergoes a dramatic increase in conductivity (over two orders of magnitude) as the rH is lowered from 21 to 1.5% (Figure 2a). This sensitivity to humidity for the device will be discussed later. Further, the shape of the conductivity curve does not change appreciably for the two humidity values (Figure 2a.1). Cooling the system from room temperature to 5 K shows a decrease in conductivity corresponding to an (Arrhenius) activation energy of 0.25 meV, two orders of magnitude lower than kT at room temperature (≈25 meV; Figure 2b). The small magnitude of activation energy confirms that at room temperature the electron transport occurs via electron tunneling.

Owing to electrostatic interaction between the negatively charged nanoparticles and positively charged PAH, the

NANO MICRO small

interparticle junction will contain PAH. Due to the hygroscopic nature of PAH, both the fiber and the interparticle junction will be soaked in water. The amount of water in the internanoparticle junctions, which depends on the ambient humidity, will regulate the device current I through the array by modulating the junction's dielectric constant. For 25 μm fiber a two orders of magnitude increase in conductivity with decreasing humidity is observed (Figure 2a.1). Decrease in humidity lowers the water content in the PAH containing the interparticle junction due to a decrease in the tunneling barrier and thus the resistance (**Figure 3**). Similarly, a device with 7 μm fiber at a bias of 1 V shows an increase in conductivity by ≈50-fold as the rH changes from 40 to 1.5%. The change in conductivity as a function of rH during the up-ramp versus down-ramp cycle is identical (Figure 3), thereby indicating that the device exhibits no hysteresis. The inset in Figure 3 a shows the field-emission SEM image of a 7-μm-thick fiber with gold nanoparticles laid across the 7-μm-wide gold electrodes. Thus, the vapor pressure of water in the surroundings, $P_v = (H/100)P^{sat}$, where H is humidity and P^{sat} is saturated vapor pressure, will regulate the device current I.

I and P_v are related as follows. As the device is sensitive to humidity at low water concentration (Figure 3 and 4), for this study, only the low ambient humidity situation is of interest. We assume that the mole fraction of water in the interparticle junction, x_J, is related to the vapor pressure at the fiber/air interface, P_i, by Roult's law (because the dissolution of water will be close to saturation), thus, $x_J = P_i/P^{sat}$. At low humidity, the mole fraction of water in the fiber, x_f, is related to P_v by Henry's law as $x_f = P_v/k_H$, where k_H is the Henry's law constant. From Roult's law between the fiber and the air, P_i is also $x_f P^{sat}$. Thus, $P_i = x_f P^{sat} = (P^{sat}/k_H)P_v$, which leads to $x_J = P_v/k_H = (P^{sat}/k_H)(H/100)$. Assuming that the effective dielectric constant follows the simple rule of mixing (with the dielectric constant of water and PAH being ≈80 and ≈3, respectively), the dielectric constant of the junction is given by $80x_J + 3(1–x_J) = 80[(P^{sat}/k_H)(H/100)] + 3[(1–(P^{sat}/k_H)(H/100)] = 0.77(P^{sat}/k_H)H + 3$. Thus, the tunneling current, I, given by the Fowler–Nordheim equation is [Equation (1)]:

$$I = \left\{ C \exp\left[-Ka\left(1 - \frac{A}{\sqrt{(0.77(P^{sat}/k_H)H + 3)}} \right)^{1/2} \right] \right\} \quad (1)$$

where:

$$K = \frac{2(2m_e)^{1/2}\phi^{1/2}}{(h)2\pi}$$

$$A = \frac{1}{\beta}\left(\frac{e^3 E}{4\pi\varepsilon_0\phi^2}\right)^{1/2}$$

where a is the average interparticle distance, m_e is the mass of the electron, ϕ is the work function of gold, e is the charge on the electron, h is Planck's constant, and E is the electric field between the nanoparticles.

To study the effect of fiber thickness on the performance of the device, three devices with different thicknesses (1, 2, and 7 μm) were investigated for their response to humidity (**Figure 4**). As expected all the devices showed an increase in conductivity with decrease in humidity at a bias voltage of 2 V with rH ranging from 1.5 to 21%. Figure 4 also shows that the Fowler–Nordheim equation [Equation (1)] fits well for these fiber devices. The total change in the conductivity for change in rH from 21 to 1.5% for 1, 2, and 7 μm fibers was ≈7.1-, 14.1-, and 30.8-fold, respectively. The fitting correlation for all devices was >0.985. The fitting parameters are shown in the inset of Figure 4. Consistent with the model, at fixed bias (i.e., fixed E), A (which is a function of material and universal constants) is remarkably constant over the

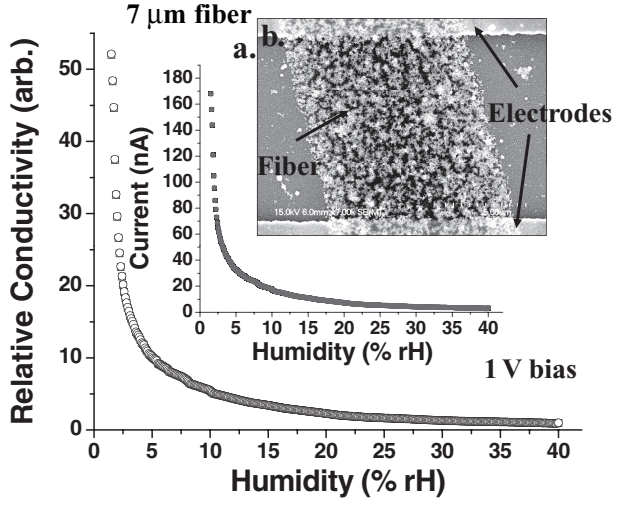

Figure 3. Relative conductivity of the device versus humidity at 1 V bias for a 7 μm fiber. There is no hysteresis when the humidity is brought back to 40% rH. Insets: a) Value of the current for the device at 1 V applied bias; b) SEM image of the 7 μm fiber spanning across the electrodes.

Fiber Size (μ)	C	Ka	a (nm)	A
1	9.83	3.42981	0.14822	2.01872
2	18.41	3.80102	0.164262	2.02885
7	59.46	5.49372	0.237412	2.01

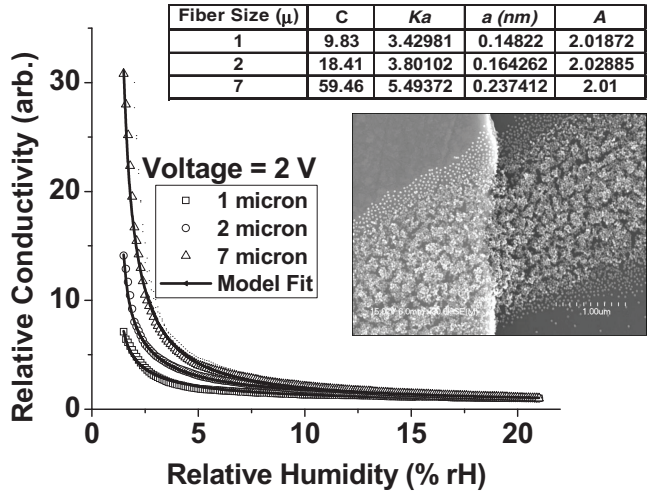

Figure 4. Relative conductivity versus humidity data and model fit for 1, 2, and 7 μm fiber devices at 2 V bias. The dark line shows the model fit. It can be seen that the model fits the data very well. The inset table shows the values of the model parameters. Inset: high-magnification SEM image showing good contact of the fiber with the gold electrode.

range of humidity values and the fiber diameters. From the *Ka* estimated from the fit and *K* defined in Equation (1), the estimated average interparticle distance *a* is estimated to be ≈0.18 nm. This value is comparable to the diameter of a PAH polymer chain of 0.16 nm, which suggests that on average there is a single monolayer of PAH between the nanoparticles through which conduction takes place. The slight increase in *a* with the fiber size is attributed to averaging over a higher number of percolating routes for electron transport. Further, the parameter *C*, which is proportional to the number of conducting channels,[32] shows a reasonably linear increase with the fiber diameter, thus indicating similar structures of the nanoparticle network on each fiber. The ≈90- and ≈7-fold change in conductivity for 25 μm fibers (Figure 2a) and 1 μm fibers (Figure 4), respectively, implies that the thicker fibers are more sensitive to humidity. Interestingly, unlike the humidity sensor built with nanoparticle deposition on bacteria,[16] there is no background or leakage current. The high-magnification SEM image in the inset in Figure 4 shows that there is good contact between the nanoparticles and gold electrode. Furthermore, all the devices produced were robust and the response was reproducible.

In another experiment, dry nitrogen was used to modulate the local humidity around the device to study the device response. On a 2 μm fiber device, dry nitrogen was switched on and off causing the current to increase and decrease, respectively (**Figure 5**a). Repeated runs indicate that switching off the nitrogen flow restores the original conductivity of the device, thus indicating high robustness and the reversible nature of water absorption/desorption at the interparticle junction. Furthermore, the sharp drop in current upon turning off the nitrogen suggests a fast response time. It is important to note that while there is a sharp change in conductivity at the beginning and the end of each humidity exposure period, there is a sluggish response in the middle. This slow response region is attributed to the slow swelling of the fiber due to water absorption, whereas the sharp response in the ends is due to adsorption/desorption on the PAH molecules between gold nanoparticles at the surface of the fiber. Further, since the fiber is expected to swell more freely in the radial direction than in the axial direction (nominally constant length), the change in interparticle tunneling distance due to swelling in the direction of the current will be minimal. We conjecture that as the diameter increases, the number of percolation paths will increase, which will in turn increase the number of tunnel junctions leading to larger sensitivity.

The response time of the device was quantified by modulating the humidity around the device by sound waves generated at particular frequencies *f* by a speaker phone installed in front of the device. The experimental setup is shown in Figure 7 of the Supporting Information. The sound modulates the pressure as $P = P_0 + \delta P = P_0 + P_A ei\ (2\pi f)t$, where P_0 is the ambient pressure, and the perturbation δP has an amplitude of P_A proportional to the sound intensity. If the water mole fraction x_0 is fixed in the perturbed region, the effective humidity changes as $H = H_0 + \delta H = H_0 + (P_A x_0/P^{sat}) ei\ (2\pi f)t$, where H_0 is the ambient, unperturbed humidity. From Equation (1), if the perturbation δH is small (as is the case for the experiment), the modulation in the device current

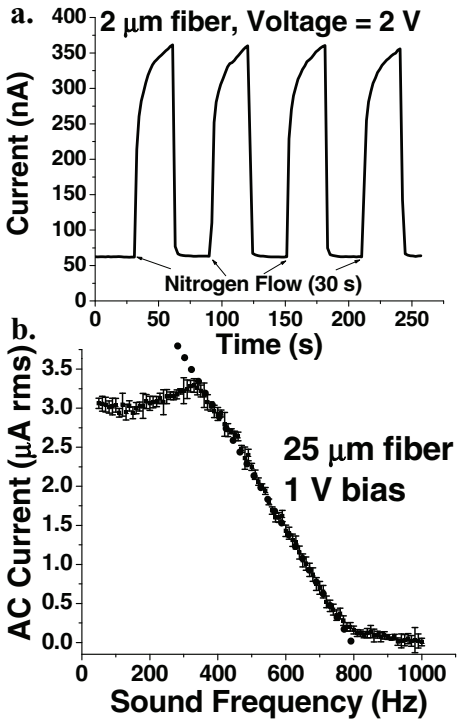

Figure 5. a) Multiple times exposure of dry N_2 gas (30 s exposure time) over a 2 μm fiber device shows the robustness of the device. The current values at 2 V bias drop fast when the N_2 is turned off showing a quick response time. b) Change in ac current response of the device with change in sound frequency, which displaces nitrogen flowing on the device. The fiber size is 25 μm and the voltage applied is 1 V. The maximum ac root-mean-square (rms) current was measured at 330 Hz (≈3.1 μA). The dotted line shows the fit for the incomplete adsorption/desorption equation.

$I = I + \delta I$ where, $\delta I = I_{ac}\ ei\ (2\pi f)t + \phi$. The amplitude of ac current I_{ac} at a fixed bias of 1 V dc was measured as a function of *f* using a lock-in amplifier. As the wavelength of the sound for the studied frequency range is >1 cm, a uniform oscillation of humidity around the device is expected that is below 20 μm. Furthermore, for high sensitivity [as seen in Figures 3 and 4, and stated in derivation of Equation (1)], only low-humidity conditions are of interest. To achieve low-humidity conditions, the sound measurements are performed under dry nitrogen flowing at ≈1 $cm^3\ s^{-1}$ over the device.

For the $f < f_{th}$, where f_{th} is the threshold frequency for mass transfer, by linearizing Equation (1) for small perturbations (i.e., $H << \delta H$), I_{ac} is independent of *f* and only depends on the experimental conditions (such as H_0, P_A, x_0, and P^{sat}) and device parameters (such as *Ka*, *A*, *C*, and bias). This condition is obtained for f < 330 Hz, where the *I*ac measured is independent of *f* (Figure 5b), thereby implying $f_{th} \approx 330$ Hz.

At $f > f_{th}$, the mass transfer becomes the rate-limiting step, since it becomes slower than the speed at which the sound wave changes the humidity. The perturbation δP_i from its equilibrium condition value of P_i is calculated by considering the flux of water from the ambient surroundings to the interface and interface to the fiber. It is reasonable to assume that

the diameter of the fiber is significantly smaller than the penetration depth of the water in PAH, thus x_f is uniform in the fiber. However, the fiber is not in equilibrium with the vapor pressure at the interface (or Roult's law is not valid), thus, $x_J \neq x_f$. Assuming an ideal law of mixing (which is reasonable for small perturbations and low humidity), the transport equation for the water concentration perturbation at the interface can be linearized as [Equation (2)]

$$\frac{d(\delta P_i)}{dt} = h[(\delta P_v) - (\delta P_i)] - \alpha(\delta P_i) \quad (2)$$

where h and α are the mass transfer coefficients for bulk-to-interface and interface-to-fiber transport, respectively. As only the first order of the perturbation (i.e., at only frequency f) is of interest, the higher-order terms leading to the $2f$, $3f$ signal can be ignored. By substituting $(\delta P_v) = x_0 P_A\, e^{i(2\pi f)t}$ and assuming the first-order term for $(\delta P_i) = P_{Ai}\, e^{i[(2\pi f)t+\phi]}$ in Equation (2), the frequency dependence of P_{Ai} is given by, $P_{Ai} \approx x_0 P_A/[(h+\alpha)^2+(2\pi f)^2]^{1/2}$. The corresponding perturbation in x_J from equilibrium, $\delta x_J = (\delta P_{Ai})/P^{sat}$. Substituting for $x_J + \delta x_J$, in Equation (1) for the change in dielectric term as $80[x_J + \delta x_J] + 3[1 - (x_J + \delta x_J)]$, the perturbation in device current, $\delta I \approx I\,(\delta x_J) e^{i[(2\pi f)t+\phi']}$, where I is the dc current with no sound exposure. As a result, from the (δx_J), the amplitude of the δI yields the amplitude of ac current as [Equation (3)]

$$I_{ac} \tilde{I} \frac{x_0 P_A}{P^{sat}} \frac{1}{(h+\alpha)^2 + (2\pi f)^2)^{1/2}} \quad (3)$$

Consistent with Figure 5b, the ac current decrease as f increases. However, as observed in Figure 5b the dependence is not linear, but quadratic. The lowering of the current with f is reasonable implying that as the frequency increases the system's response becomes increasingly incomplete. Finally, at $f > 800$ Hz the system is unable to respond to the perturbation resulting in vanishingly small ac current. Furthermore, as the sensor is in quasi-equilibrium with the surroundings to frequencies as high as 330 Hz, the sensor has a response time of $1/330 \approx 3$ ms.

The conductivity of the device was also studied for its dependence on change in air pressure. For a 25 μm fiber device, a decrease in pressure from 820 to ≈1 Torr led to a decrease in resistance from ≈100 to 35.3 MΩ (see the Supporting Information, Figure 8). Thus, another application of this device could be a local pressure gauge.

4. Conclusion

In summary, we have demonstrated an approach for *the* directed self-assembly of a molecular-junction network of gold nanoparticles on a polyelectrolyte fiber scaffold to produce a highly sensitive and ultrafast humidity sensor. The device conductivity changes by two orders of magnitude in response to a decrease in humidity from 21 to 1.5%. The modulation of humidity due to an acoustic pressure wave showed that the response time of the device is at least 3 ms. The approach can potentially be extended to designing more sophisticated sensors and molecular electronics devices with specificity defined by the chemistry of the polymer and functionalization on the nanoparticles.

Supporting Information

Supporting Information is available from the Wiley Online Library or from the author.

Acknowledgements

R.F.S. would like to thank the National Science Foundation (NER/CMMI 608877) for financial support. We would like to thank Dr. Rajinder Gill for help in making the fiber by electrospinning.

[1] Y. Cui, X. F. Duan, J. T. Hu, C. M. Lieber, *J. Phys. Chem. B* **2000**, *104*, 5213–5216.
[2] Y. Cui, C. M. Lieber, *Science* **2001**, *291*, 851–853.
[3] Y. Cui, Q. Q. Wei, H. K. Park, C. M. Lieber, *Science* **2001**, *293*, 1289–1292.
[4] G. F. Zheng, W. Lu, S. Jin, C. M. Lieber, *Adv. Mater.* **2004**, *16*, 1890–1893.
[5] K. K. Likharev, *Proc. IEEE* **1999**, *87*, 606–632.
[6] H. Cai, C. Xu, P. G. He, Y. Z. Fang, *J. Electroanal. Chem.* **2001**, *510*, 78–85.
[7] G. Canziani, W. T. Zhang, D. Cines, A. Rux, S. Willis, G. Cohen, R. Eisenberg, I. Chaiken, *Methods* **1999**, *19*, 253–269.
[8] P. Hanarp, D. S. Sutherland, J. Gold, B. Kasemo, *Colloids Surf. A* **2003**, *214*, 23–36.
[9] M. J. Wang, C. Y. Sun, L. Y. Wang, X. H. Ji, Y. B. Bai, T. J. Li, J. H. Li, *J. Pharm. Biomed. Anal.* **2003**, *33*, 1117–1125.
[10] F. Patolsky, G. F. Zheng, C. M. Lieber, *Anal. Chem.* **2006**, *78*, 4260–4269.
[11] J. R. Heath, *Pure Appl. Chem.* **2000**, *72*, 11–20.
[12] A. N. Korotkov, K. K. Likharev, *J. Appl. Phys.* **1998**, *84*, 6114–6126.
[13] V. P. Roychowdhury, D. B. Janes, S. Bandyopadhyay, *Proc. IEEE* **1997**, *85*, 574–588.
[14] V. Berry, A. Gole, S. Kundu, C. J. Murphy, R. F. Saraf, *J. Am. Chem. Soc.* **2005**, *127*, 17600–17601.
[15] V. Berry, S. Rangaswamy, R. F. Saraf, *Nano Lett.* **2004**, *4*, 939–942.
[16] V. Berry, R. F. Saraf, *Angew. Chem. Int. Ed.* **2005**, *44*, 6668–6673.
[17] D. Schubert, R. Dargusch, J. Raitano, S. W. Chan, *Biochem. Biophys. Res. Commun.* **2006**, *342*, 86–91.
[18] M. Das, S. Patil, N. Bhargava, J. F. Kang, L. M. Riedel, S. Seal, J. J. Hickman, *Biomaterials* **2007**, *28*, 1918–1925.
[19] T. R. Pisanic, J. D. Blackwell, V. I. Shubayev, R. R. Finones, S. Jin, *Biomaterials* **2007**, *28*, 2572–2581.
[20] S. Ghosh, A. K. Sood, N. Kumar, *Science* **2003**, *299*, 1042–1044.
[21] C. S. Park, B. S. Kang, D. W. Lee, T. Y. Choi, Y. S. Choi, *Microelectron. Eng.* **2007**, *84*, 1316–1319.
[22] Z. L. Wang, J. H. Song, *Science* **2006**, *312*, 242–246.
[23] F. Patolsky, G. F. Zheng, C. M. Lieber, *Anal. Chem.* **2006**, *78*, 4260–4269.
[24] S. J. Tans, A. R. M. Verschueren, C. Dekker, *Nature* **1998**, *393*, 49–52.

[25] K. Yano, T. Ishii, T. Hashimoto, T. Kobayashi, F. Murai, K. Seki, *IEEE Trans. Electron Devices* **1994**, *41*, 1628–1638.
[26] J. Chen, M. A. Reed, A. M. Rawlett, J. M. Tour, *Science* **1999**, *286*, 1550–1552.
[27] N. P. Guisinger, R. Basu, A. S. Baluch, M. C. Hersam, *Ann. N.Y. Acad. Sci.* **2003**, *1006*, 227–234.
[28] M. Shin, S. J. Lee, K. W. Park, E. Lee, *J. Appl. Phys.* **1998**, *84*, 2974–2976.
[29] E. Arici, D. Meissner, F. Schaffler, N. S. Sariciftci, *Int. J. Photoenergy* **2003**, *5*, 199–208.
[30] T. Hasobe, H. Imahori, P. V. Kamat, T. K. Ahn, S. K. Kim, D. Kim, A. Fujimoto, T. Hirakawa, S. Fukuzumi, *J. Am. Chem. Soc.* **2005**, *127*, 1216–1228.
[31] K. T. Nam, D. W. Kim, P. J. Yoo, C. Y. Chiang, N. Meethong, P. T. Hammond, Y. M. Chiang, A. M. Belcher, *Science* **2006**, *312*, 885–888.
[32] V. Maheshwari, R. F. Saraf, *Science* **2006**, *312*, 1501–1504.

Received: March 17, 2011
Published online:

